

Reentrant stability of superconducting films and the vanishing of dendritic flux instability

V. V. Yurchenko, D. V. Shantsev, and T. H. Johansen

*Department of Physics and Center for Materials Science and Nanotechnology, University of Oslo,
P.O. Box 1048, Blindern, 0316 Oslo, Norway*

M. R. Nevala and I. J. Maasilta

Nanoscience Center, Department of Physics, University of Jyväskylä, P.O. Box 35, FIN 40014, Finland

K. Senapati and R. C. Budhani

Department of Physics, Indian Institute of Technology Kanpur, Kanpur 208016, India

(Received 20 August 2007; published 26 September 2007)

We propose a mechanism responsible for the abrupt vanishing of the dendritic flux instability found in many superconducting films when an increasing magnetic field is applied. The onset of flux avalanches and the subsequent reentrance of stability in NbN films were investigated using magneto-optical imaging, and the threshold fields were measured as functions of critical current density j_c . The results are explained with excellent quantitative agreement by a thermomagnetic model published recently [D. V. Denisov *et al.*, Phys. Rev. B **73**, 014512 (2006)], showing that the reentrant stability is a direct consequence of a monotonously decreasing j_c versus field.

DOI: [10.1103/PhysRevB.76.092504](https://doi.org/10.1103/PhysRevB.76.092504)

PACS number(s): 74.25.Qt, 68.60.Dv, 74.25.Ha, 74.78.Db

In most superconductors, a slow increase of external magnetic field is accompanied by a gradual penetration of magnetic vortices, which makes their way into the sample through a random energy landscape created by structural irregularities. This results in formation of a critical state characterized by a critical gradient of the vortex density corresponding to the maximum lossless current in the superconductor.¹ The critical state, however, is metastable and can be destroyed by flux jumps where large-scale redistribution of the vortices suddenly takes place. Such dramatic events, observed experimentally as abrupt drops in the magnetization, are due to a thermomagnetic instability where the local dissipation associated with vortex motion reduces the pinning, which in turn facilitates further motion.² With this positive feedback, a small perturbation can quickly evolve into a flux avalanche of sample spanning dimensions.

In recent years, space-resolved measurements, in particular, using magneto-optical imaging (MOI), have revealed the detailed morphology of flux avalanches. Most work was carried out on superconducting thin films of MgB₂,³⁻⁷ Nb,^{8,9} Pb,¹⁰ Nb₃Sn,¹¹ NbN,¹² YBa₂Cu₃O_x,^{13,14} and YNi₂B₂C,¹⁵ where the images show that a typical flux avalanche in superconducting films has a branched dendritic structure with 50–100 μm wide branches. While each avalanche event has only local impact, they occur very frequently, i.e., with very small applied field intervals, and therefore manifest in magnetization versus field curves as a strong noisy component.^{3,5,12,15-17}

These magnetization curves also display two other generic features, namely, the existence of a threshold field for the onset of avalanche activity, typically at a few millitesla, and an upper threshold field above which the superconductor regains full stability. In a recent letter,¹⁸ we reported a detailed study of the lower threshold and explained key features of the instability onset. The important question why superconducting films suddenly become stable again at high fields remains open and is the focus of the present work. We

report here experiments carried out on films of superconducting NbN and discuss the results within the theoretical framework of a recently proposed thermomagnetic model.^{19,20} The reentrant stability is explained by accounting for the field dependence of the critical current density.

Superconducting films of NbN were prepared on single crystal (100) MgO substrates by pulsed laser ablation of a high purity Nb target in a controlled ultrahigh purity (99.9996) N₂ environment. A KrF excimer laser (248 nm) operated at 20 Hz was used for ablation with pulse energy density of 5 J/cm² on the target surface. Detailed procedures and structural characterization of the samples, which are superconducting below $T_c=15$ K, are found in Ref. 21. The films have a thickness of $d=280$ nm and were lithographically patterned into a rectangular shape 2.4 mm wide and 4.8 mm long using reactive ion etching in a CHF₃+O₂ plasma.

Flux penetration into the samples was investigated using a MOI method based on the Faraday effect in an in-plane magnetized bismuth-substituted ferrite garnet sensor film that was placed on top of the NbN film. The sample was mounted on the cold finger of a continuous He-flow cryostat (Microstat, Oxford), which in turn was placed under the objective lens of a reflected light polarizing microscope (Leica). A variable magnetic field was applied perpendicular to the sample using a pair of resistive coils. The microscope was equipped with a mercury lamp, and by using crossed polarizers, the resulting image brightness represents the local magnitude of the perpendicular flux density.

Shown in Fig. 1 is a set of images recorded during a slow ramping up of the applied magnetic field H after the sample was initially zero-field cooled to $T=4$ K. In image (a), taken at $H=8$ Oe, there is only a shallow penetration, with a flux front that moved gradually inward as the field increased. This smooth mode of penetration ended abruptly when reaching $H=12$ Oe, where a flux avalanche suddenly occurred. The avalanche area is seen in Fig. 1 taken at 12 Oe as the branch-

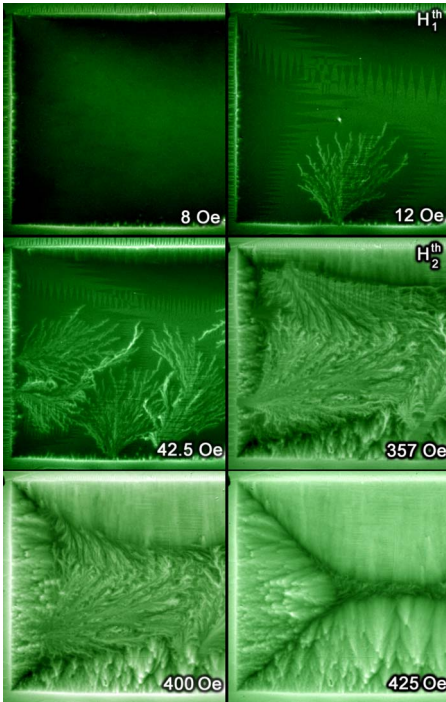


FIG. 1. (Color online) Magneto-optical images of a NbN film (only the left half of the sample area is shown) at 4 K in increasing applied field. The left edge of the sample, seen as a vertical line of enhanced brightness, is 2.4 mm long. The images were contrast enhanced individually.

ing structure rooted on the lower sample edge. As the applied field increased further, more and more avalanches took place, creating a complex pattern of flux dendrites covering most of the sample area (see Fig. 1 at $H=42.5$ Oe). Then, as the field reached $H=357$ Oe, the avalanche activity stopped entirely although the field continued to increase. The advancing flux front now erased the previously formed dendritic structures (see Fig. 1 at $H=400$ and 425 Oe), and the critical-state mode of flux penetration was restored. The bright fanlike features in the lower part of the images are due to tiny film defects and are not related to the flux instability.

This experiment gives direct evidence that there exists an upper threshold field for the dendritic instability, in agreement with earlier measurements on various superconducting films.^{3,12,15,16} Before presenting more results, we first give a qualitative argument for why reentrant stability can follow from the thermomagnetic model proposed in Ref. 20. The theory predicts that a superconducting thin strip of half-width w becomes unstable when the flux penetration depth exceeds

$$\ell^* = \frac{\pi}{2} \sqrt{\frac{\kappa T^*}{j_c E}} \left(1 - \sqrt{\frac{2h_0 T^*}{n d j_c E}} \right)^{-1}, \quad (1)$$

provided that $\ell^* < w$. Here, j_c is the critical current density, $T^* \equiv -(\partial \ln j_c / \partial T)^{-1}$, E is the electric field, κ is the thermal conductivity, and h_0 is the coefficient of heat transfer from the superconducting film to the substrate. The parameter n characterizes the nonlinearity of the current-voltage curve of

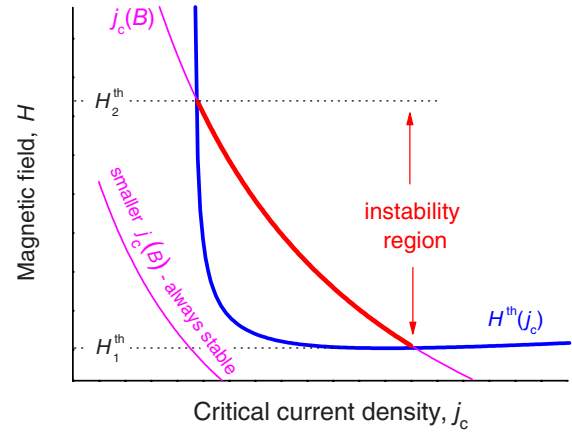


FIG. 2. (Color online) Schematic plot illustrating the existence of two threshold fields for the dendritic instability. The two main curves represent the threshold field H^{th} versus j_c according to Eqs. (1) and (2) and a typical monotonous field dependence of the critical current density. The intersection of the two curves defines the two thresholds H_1^{th} and H_2^{th} for the onset and vanishing of the instability.

the superconductor, $n = \partial \ln E / \partial \ln j \gg 1$. The instability onset field can be obtained from ℓ^* using the Bean model relation between the penetration depth and applied field,²⁵

$$H^{\text{th}} = \frac{j_c d}{\pi} \operatorname{arccosh} \left(\frac{w}{w - \ell^*} \right). \quad (2)$$

It follows from Eqs. (1) and (2) that the threshold field depends strongly on the critical current density, more specifically according to the graph marked $H^{\text{th}}(j_c)$ in Fig. 2. For intermediate j_c , the threshold field is nearly constant and increases slowly as j_c becomes larger, giving eventually a sub-linear asymptotic dependence, $H^{\text{th}} \sim j_c^{3/4}$. More importantly, when j_c decreases, the threshold field will diverge at some finite j_c , corresponding to $\ell^*(j_c)$ approaching w . Taking now into account that the critical current density most commonly decreases with the field, typically as the $j_c(B)$ curve in Fig. 2, it follows that the field range with unstable behavior can indeed have both a lower and an upper limit, H_1^{th} and H_2^{th} , as indicated in the figure. Evidently, it is essential in this picture how fast j_c is decreasing with the field. For example, in the Bean model (constant j_c), or with a j_c having only weak field dependence, the conditions for having an upper threshold will never be met. Note also that if j_c is sufficiently small, e.g., because of a larger temperature, the thermomagnetic avalanches will not occur at any magnetic field.

To obtain quantitative support for this explanation, we performed MOI of flux penetration after first cooling the sample to 4 K in various constant magnetic fields, H_{fc} . This allowed measurement of the field dependence of both j_c and the two instability threshold fields. Cooling fields up to 300 Oe were applied, and MOI did not detect any contrast, which implies that the full flux density H_{fc} was frozen into the sample. To measure j_c , a small additional field was subsequently applied, creating a critical-state type of penetration of the new flux.²⁶ From the depth of the penetration front in

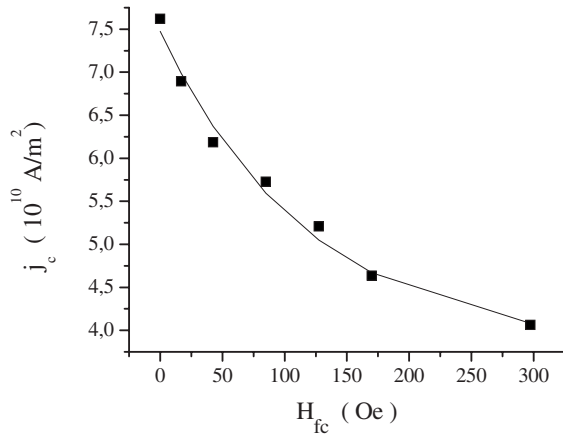


FIG. 3. Field dependence of the critical current density at $T = 4$ K measured using MOI.

the middle section of the rectangular sample, the j_c was determined,^{26,27} and Fig. 3 shows its dependence on the cooling field. A nearly exponential decay was found, with j_c decreasing from 7.6×10^{10} A m⁻² at zero field to almost one-half at $H_{fc} = 300$ Oe. This agrees well with the results obtained earlier from ac susceptibility measurements²¹ on the same type of films.

The threshold fields were determined by slowly ramping up the additional field after an initial field cooling. The values of the total applied field when the first and last flux dendrites appeared were recorded for various H_{fc} , giving the result shown in Fig. 4. The onset field increases almost linearly and with some upward curvature, whereas the upper threshold field remains essentially constant until the two thresholds eventually merge into one when $H_{fc} = 300$ Oe. For larger cooling fields, i.e., for smaller j_c 's, the instability was found to be fully suppressed.

To demonstrate that these data are in excellent agreement

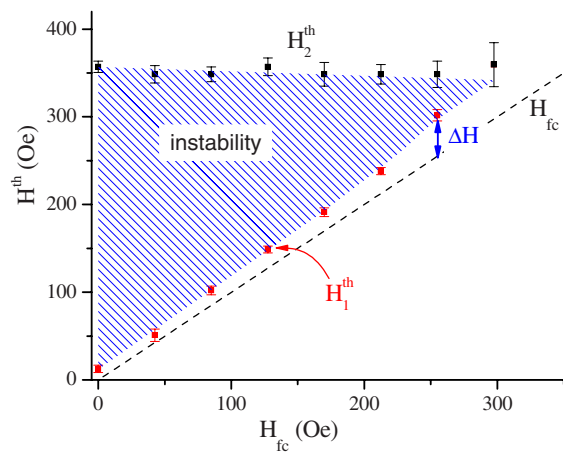


FIG. 4. (Color online) The lower and upper threshold fields H_1^{th} (disks) and H_2^{th} (triangles) measured at different frozen-in fields after field cooling to 4 K. The hatched area indicates the region of unstable behavior. The upper boundary has a slope where the high-field end point lies 14 Oe below the zero-field value, as predicted by the model.

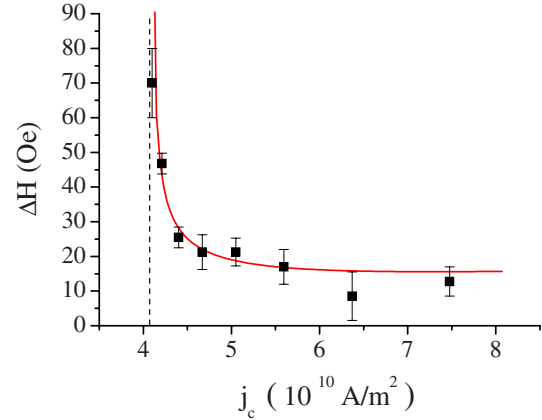


FIG. 5. (Color online) Instability onset field ΔH as a function of the critical current at 4 K. The plot shows experimental data (squares) and a theoretical prediction (full line) using fitting parameters given in the text. This plot made use also of the experimental data in Fig. 3 to convert from H_{fc} to j_c . The error bars indicate the spread in the data obtained by repeating the experiments several times.

with the scenario depicted in Fig. 2, we first note that the applied field which induces shielding currents in the sample, and triggers the first avalanche, is $\Delta H = H_1^{\text{th}} - H_{fc}$. Thus, in the presence of a cooling field, the curve representing the $H^{\text{th}}(j_c)$ in Fig. 2 should be shifted upward by the amount H_{fc} , while the $j_c(B)$ curve remains as is. Then, as H_{fc} becomes larger, the distance between the two intersection points of the curves becomes gradually smaller, and at some cooling field, the two thresholds become one, just like in the experiments. To show the agreement quantitatively, the data for the lower threshold field are replotted in Fig. 5 as ΔH versus j_c . The full curve is a theoretical curve obtained from Eqs. (1) and (2) using two fitting parameters, $\kappa T^*/E = 500$ mA and $h_0 T^*/nE = 5700$ A/m (which can mean, e.g., $\kappa = 25$ mW/K m, $h_0 = 1424$ W/K m², $n = 5$, $E = 0.55$ V/m, $T^* = 11$ K).

In contrast to H_1^{th} , the upper threshold field H_2^{th} was found to be essentially independent of H_{fc} . Even this behavior is fully consistent with our explanation illustrated by Fig. 2. Near the intersection point determining H_2^{th} , the diverging $H^{\text{th}}(j_c)$ curve has a very steep slope. Hence, a vertical shift of $H^{\text{th}}(j_c)$ accounting for a nonzero cooling field H_{fc} hardly changes the value of H_2^{th} . The robustness of the upper threshold field by being independent of the initial conditions is actually a remarkable and unexpected result. Indeed, the flux distribution after cooling the sample in H_{fc} and then ramping the field up to H_2^{th} dramatically depends on the value of H_{fc} . In the zero-field cooled experiment shown in Fig. 1, one finds dozens of overlapping dendrites, while for $H_{fc} = 300$ Oe, the flux distribution remains of a critical-state type until a single dendritic structure is formed at H_2^{th} . Note that the exact dendritic pattern is every time different even if one repeats the experiment under the same conditions. Thus, despite the wide variety of flux distributions, the dendritic activity in all these cases vanishes at the *same* threshold field $H_2^{\text{th}} \approx 350$ Oe. Note also that the $H^{\text{th}}(j_c)$ curve in Fig. 2 was

calculated²⁰ assuming an initial critical-state flux distribution, and therefore the observed invariance of H_2^{th} suggests that the theoretical prediction is valid for a much broader set of initial magnetic states.

The present thermomagnetic scenario, and, in particular, the $H^{\text{th}}(j_c)$ dependence shown in Fig. 2, has very recently received even further support from MOI studies of MgB_2 films grown on vicinal substrates giving a slight anisotropy in the critical current.²⁴ The observed dramatic anisotropy in the direction of dendritic avalanches was fully explained by the very steep slope of the $H^{\text{th}}(j_c)$ curve.

In conclusion, the dendritic flux instability, which is a serious threat to superconducting devices based on thin films,

was investigated to understand mechanisms that allow the films to recover stability. We explained reentrant stability in the framework of a thermomagnetic model²⁰ and demonstrated by a quantitative agreement of the theory with experimental results that it stems from the field dependence of the critical current.

This work was supported by the Research Council of Norway, Grant No. 158518/431 (NANOMAT). Research at IIT Kanpur has been supported by a grant from the Council of Scientific and Industrial Research (CSIR), Government of India. The authors acknowledge fruitful discussions with D. G. Gheorghe and R. J. Wijngaarden.

-
- ¹C. P. Bean, *Rev. Mod. Phys.* **36**, 31 (1964).
²R. G. Mints and A. L. Rakhmanov, *Rev. Mod. Phys.* **53**, 551 (1981).
³T. H. Johansen, M. Baziljevich, D. V. Shantsev, P. E. Goa, Y. M. Galperin, W. N. Kang, H. J. Kim, E. M. Choi, M.-S. Kim, and S. I. Lee, *Europhys. Lett.* **59**, 599 (2002).
⁴F. L. Barkov, D. V. Shantsev, T. H. Johansen, P. E. Goa, W. N. Kang, H. J. Kim, E. M. Choi, and S. I. Lee, *Phys. Rev. B* **67**, 064513 (2003).
⁵Z. X. Ye, Q. Li, Y. F. Hu, A. V. Pogrebnyakov, Y. Cui, X. X. Xi, J. M. Redwing, and Q. Li, *Appl. Phys. Lett.* **85**, 5284 (2004).
⁶J. Albrecht, A. T. Matveev, M. Djupmyr, G. Schutz, B. Stuhlhofer, and H.-U. Habermeier, *Appl. Phys. Lett.* **87**, 182501 (2005).
⁷F. Laviano, D. Botta, C. Ferdeghini, V. Ferrando, L. Gozzelino, and E. Mezzetti, in *Magneto-Optical Imaging*, edited by T. H. Johansen and D. Shantsev (Kluwer Academic, Dordrecht, 2004), p. 237.
⁸C. A. Duran, P. L. Gammel, R. E. Miller, and D. J. Bishop, *Phys. Rev. B* **52**, 75 (1995).
⁹M. S. Welling, R. J. Westerwaal, W. Lohstroh, and R. J. Wijngaarden, *Physica C* **411**, 11 (2004).
¹⁰M. Menghini, R. J. Wijngaarden, A. V. Silhanek, S. Raedts, and V. V. Moshchalkov, *Phys. Rev. B* **71**, 104506 (2005).
¹¹I. A. Rudnev, S. V. Antonenko, D. V. Shantsev, T. H. Johansen, and A. E. Primenko, *Cryogenics* **43**, 663 (2003).
¹²I. A. Rudnev, D. V. Shantsev, T. H. Johansen, and A. E. Primenko, *Appl. Phys. Lett.* **87**, 042502 (2005).
¹³P. Leiderer, J. Boneberg, P. Brull, V. Bujok, and S. Herminghaus, *Phys. Rev. Lett.* **71**, 2646 (1993).
¹⁴B. Biehler, B.-U. Runge, P. Leiderer, and R. G. Mints, *Phys. Rev. B* **72**, 024532 (2005).
¹⁵S. C. Wimbush, B. Holzapfel, and Ch. Jooss, *J. Appl. Phys.* **96**, 3589 (2004).
¹⁶Z. W. Zhao, S. L. Li, Y. M. Ni, H. P. Yang, Z. Y. Liu, H. H. Wen, W. N. Kang, H. J. Kim, E. M. Choi, and S. I. Lee, *Phys. Rev. B* **65**, 064512 (2002).
¹⁷S. Jin, H. Mavoori, C. Bower, and R. B. van Dover, *Nature (London)* **411**, 563 (2001).
¹⁸D. V. Denisov, D. V. Shantsev, Y. M. Galperin, E.-M. Choi, H.-S. Lee, S.-Ik Lee, A. V. Bobyl, P. E. Goa, A. A. F. Olsen, and T. H. Johansen, *Phys. Rev. Lett.* **97**, 077002 (2006).
¹⁹I. S. Aranson, A. Gurevich, M. S. Welling, R. J. Wijngaarden, V. K. Vlasko-Vlasov, V. M. Vinokur, and U. Welp, *Phys. Rev. Lett.* **94**, 037002 (2005).
²⁰D. V. Denisov, A. L. Rakhmanov, D. V. Shantsev, Y. M. Galperin, and T. H. Johansen, *Phys. Rev. B* **73**, 014512 (2006).
²¹K. Senapati, N. K. Pandey, R. Nagar, and R. C. Budhani, *Phys. Rev. B* **74**, 104514 (2006).
²²M. Baziljevich, A. V. Bobyl, D. V. Shantsev, E. Altshuler, T. H. Johansen, and S. I. Lee, *Physica C* **369**, 93 (2002).
²³E.-M. Choi, H.-S. Lee, H. J. Kim, B. Kang, S.-Ik Lee, A. A. F. Olsen, D. V. Shantsev, and T. H. Johansen, *Appl. Phys. Lett.* **87**, 152501 (2005).
²⁴J. Albrecht, A. T. Matveev, J. Stempfer, H.-U. Habermeier, D. V. Shantsev, Y. M. Galperin, and T. H. Johansen, *Phys. Rev. Lett.* **98**, 117001 (2007).
²⁵E. H. Brandt and M. Indenbom, *Phys. Rev. B* **48**, 12893 (1993).
²⁶To avoid flux dendrite formation in these experiments, the superconductor was placed in close contact with the metallic mirror of the garnet sensor film, which is known to suppress the instability (Refs. 22 and 23).
²⁷A more precise way to determine $j_c(B)$ should be based on the self-consistent relation between the penetration depth and the $j_c(B)$ law derived in J. McDonald and J. R. Clem, *Phys. Rev. B* **53**, 8643 (1996).